HHS Public Access

Author manuscript

Glia. Author manuscript; available in PMC 2023 March 01.

Published in final edited form as:

Glia. 2022 March ; 70(3): 508–521. doi:10.1002/glia.24119.

Dilation of cortical capillaries is not related to astrocyte calcium signaling

Armani P. Del Franco, **Pei-Pei Chiang**, **Eric A. Newman**

Department of Neuroscience, University of Minnesota, Minneapolis, MN, USA

Abstract

The brain requires an adequate supply of oxygen and nutrients to maintain proper function as neuronal activity varies. This is achieved, in part, through neurovascular coupling mechanisms that mediate local increases in blood flow through the dilation of arterioles and capillaries. The role of astrocytes in mediating this functional hyperemia response is controversial. Specifically, the function of astrocyte Ca^{2+} signaling is unclear. Cortical arterioles dilate in the absence of astrocyte Ca^{2+} signaling, but previous work suggests that Ca^{2+} increases are necessary for capillary dilation. This question has not been fully addressed in vivo, however, and we have reexamined the role of astrocyte Ca^{2+} signaling in vessel dilation in the barrel cortex of awake, behaving mice. We recorded evoked vessel dilations and astrocyte Ca^{2+} signaling in response to whisker stimulation. Experiments were carried out on WT and IP3R2 KO mice, a transgenic model where astrocyte Ca^{2+} signaling is substantially reduced. Compared to WT mice at rest, Ca^{2+} signaling in astrocyte endfeet contacting capillaries increased by 240% when whisker stimulation evoked running. In contrast, Ca^{2+} signaling was reduced to 9% of WT values in IP3R2 KO mice. In all three conditions, however, the amplitude of capillary dilation was largely unchanged. In addition, the latency to the onset of astrocyte Ca^{2+} signaling lagged behind dilation onset in most trials, although a subset of rapid onset Ca^{2+} events with latencies as short as 0.15 s occurred. In summary, we found that whisker stimulation-evoked capillary dilations occurred independent of astrocyte Ca^{2+} increases in the cerebral cortex.

Graphical Abstract

CONFLICT OF INTEREST. The authors declare no conflict of interest.

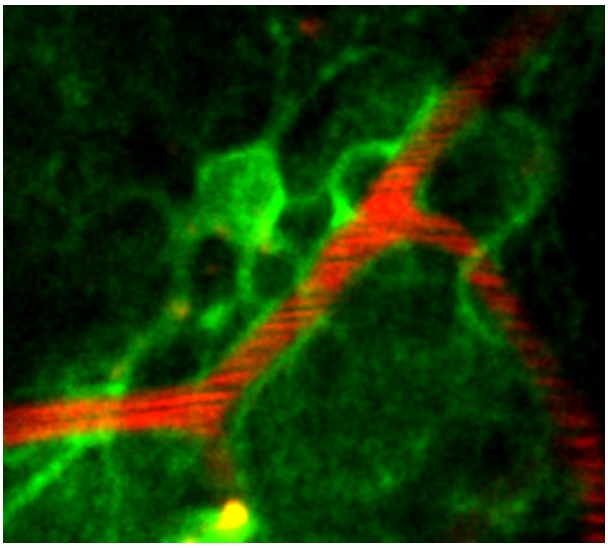

Keywords

Astrocyte; calcium signaling; capillary dilation; cerebral blood flow; IP3R2 KO; awake mouse; endfeet; processes

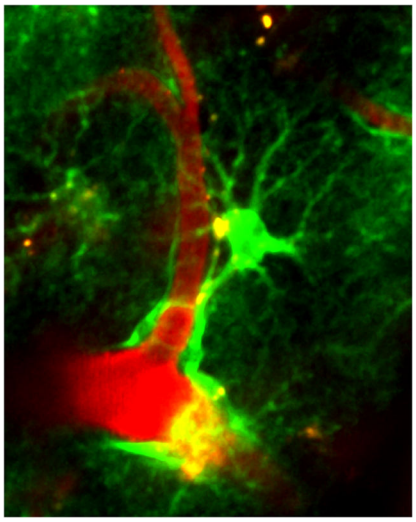

Two-photon microscopy image of an astrocyte enveloping a capillary that is branching off of a penetrating arteriole (bottom) in the somatosensory cortex of the awake mouse. Astrocytes are labeled with GCaMP6f (green) and blood vessels are filled with Texas Red dextran (red).

INTRODUCTION

Multiple regulatory mechanisms ensure that the brain receives an adequate supply of oxygen and nutrients as the metabolic demands of its neurons vary. Among these mechanisms is functional hyperemia. Focal increases in neuronal activity result in localized increases in blood flow to active brain regions (Attwell et al., 2010; Mishra et al., 2021). Increases

in blood flow are generated by dilation of arteries on the surface of the brain as well as arterioles and capillaries within the brain. This response is the basis of blood oxygen level-dependent functional imaging (BOLD fMRI) (Mishra et al., 2021). Several signaling mechanisms mediate vessel dilation in response to increased neuronal activity. These neurovascular coupling mechanisms include direct signaling from neurons to blood vessels and indirect signaling via astrocytes and vascular endothelial cells acting as relay cells (Attwell et al., 2010; Nippert et al., 2018; Pfeiffer et al., 2021). Direct neuronal signaling to vessels can be mediated by release of nitric oxide (NO) and prostaglandins. Indirect signaling via astrocytes may be mediated by release of prostaglandins, epoxyeicosatrienoic acids (EETs), and K^+. Endothelial cells may also release vasodilatory signals in response to neuronal activity. These neurovascular coupling mechanisms work in concert, but the importance of individual mechanisms may vary in different brain regions and under different physiological and pathological conditions and their relative contribution to vessel dilation remains a matter of debate.

One ongoing controversy concerns astrocyte-mediated vessel dilation and, in particular, whether activity-dependent increases in Ca^{2+} within astrocytes mediate vessel dilation. Inositol-trisphosphate receptor 2 knockout (IP3R2 KO) mice have been particularly useful in addressing this question. The IP3R2 receptor is expressed exclusively in astrocytes in the CNS and is responsible for most Ca^{2+} signaling in these glial cells (Holtzclaw et al., 2002). Ca^{2+} signaling in astrocytes is largely, but not completely eliminated in IP3R2 KO animals (Srinivasan et al., 2015; Stobart et al., 2018). However, stimulus-evoked arteriole dilation is not diminished in these KO animals (Nizar et al., 2013; Takata et al., 2013; Bonder and McCarthy, 2014; Biesecker et al., 2016). Even in WT animals, arteriole dilations are observed in the absence of astrocyte Ca^{2+} signaling or, if Ca^{2+} increases are seen, they occur following dilation (Nizar et al., 2013; Bonder and McCarthy, 2014; Tran et al., 2018). These observations indicate that arteriole dilation is not mediated by astrocyte Ca^{2+} signaling. However, this conclusion has been challenged by recent observations demonstrating rapid stimulus-evoked Ca^{2+} increases in astrocytes in WT and IP3R2 KO animals (Lind et al., 2013; Otsu et al., 2015; Stobart et al., 2018).

Capillaries as well as arterioles within the brain actively dilate in response to neuronal activity and contribute to functional hyperemia (Hall et al., 2014; Attwell et al., 2016; Khennouf et al., 2018). The importance of astrocyte Ca^{2+} signaling in mediating capillary dilation may differ from that of arteriole dilation. In cortical brain slices, buffering astrocyte Ca^{2+} increases with BAPTA substantially reduces electrical stimulus-evoked capillary dilations, but not arteriole dilations (Mishra et al., 2016). Similarly, in the retina, light-evoked vasodilations are blocked in capillaries but not in arterioles when evoked Ca^{2+} increases are reduced in Müller cells (the principal macroglial cells of the retina) in IP3R2 KO animals (Biesecker et al., 2016). Ca^{2+} increases are both necessary and sufficient to evoke capillary dilations in the retina. These results suggest that unlike arterioles, capillary dilations are mediated by Ca^{2+} signaling in astrocytes. However, this question has not been fully addressed in vivo using physiological stimuli.

We have reexamined the role of astrocyte Ca^{2+} signaling in neurovascular coupling in the barrel cortex utilizing awake behaving mice. We anticipated that whisker stimulation-

evoked capillary dilations would be abolished in IP3R2 KO animals. Instead, we found that capillary dilations as well as arteriole dilations were not reduced in the absence of evoked Ca^{2+} increases. Whisker stimulation evoked capillary dilations in 1st through 4th order capillaries in both WT and KO animals, indicating that capillary dilation in the cortex is not related to astrocyte Ca^{2+} signaling.

METHODS

Ethics Statement

All experimental procedures were approved by and adhered to the guidelines of the Institutional Animal Care and Use Committee of the University of Minnesota.

Animals

All experiments were performed on 8 – 20 week old male and female IP3R2$^{-/-}$ and WT littermate mice on a C57BL/6 background (Jackson Lab #000664) obtained from Dr. J. Chen, University California, San Diego, La Jolla, CA.

Viral transfection

Astrocyte Ca^{2+} signaling was monitored with both cytoplasmic and membrane-tethered GCaMP6f induced by viral transfection. pZac2.1 gfaABC1D-cyto-GCaMP6f (Addgene plasmid #52925) and pZac2.1 gfaABC1D-lck-GCaMP6f were from Baljit Khakh (Addgene viral prep # 52924-AAV5) and packaged into AAV serotype 5 by the University of Minnesota Viral Vector Core and Addgene, respectively. The promoter and serotype were chosen for selective GCaMP6f expression in astrocytes (Srinivasan et al., 2016).

Surgery and Virus Injection

Surgical methods were adopted from Tran and Gordon (Tran and Gordon, 2015). Dexamethosane (2mg/kg, S.C.) and SR-Buprenex (2mg/kg, S.C.) were administered prior to surgery and mice were anesthetized with isoflurane (4% induction, 1.5% maintenance). The bregma, lambda and sagittal sutures were exposed and a titanium headbar was secured to the frontal and parietal bones with cyanoacrylate glue and two screws (F000CE094, J.I. Morris). A 3 mm diameter craniotomy over the left whisker barrel cortex was performed while keeping the dura intact. 750 to 1000 nL of either AAV5-gfaABC1D-Cyto-GCaMP6f (1×10^{13} particles/mL) or AAV5-gfaABC1D-Lck-GCaMP6f (1×10^{12} particles/mL) was injected into the barrel cortex 350 to 500 μm beneath the surface. AAV was injected through a glass micropipette (35 to 50 μm tip diameter) at 250 nL/min (Goldey et al., 2014). The cranial window was then rinsed with saline to remove excess blood and the craniotomy covered with a glass coverslip plug (two 3 mm diameter and one 5mm diameter glass coverslips stacked and glued together) and glued into place with cyanoacrylate glue. The glass window and the headbar were further secured with dental cement (C&B-Metabond, Parkell). After surgery, animals were given prophylactic antibiotic treatment of Sulfatrim (1:32) in drinking water for seven days.

Cortical imaging

Three weeks after surgery, mice underwent two days of acclimation on a treadmill used in the imaging experiments. Mice were secured by their headbar to the treadmill for 30 min sessions while receiving intermittent puffs of air (10 PSI) directed at their whiskers. Imaging experiments were performed four to seven weeks after surgery and viral injection. Prior to an experimental session, mice were injected with 0.05 mL of 3% (W/V) Texas Red dextran (70 kDA; Invitrogen #D1830) through the tail vein to label vessels for imaging. Mice were then secured by their headbar and imaged with a custom-built two-photon laser scanning (2P) microscope and a 16X, 0.8 NA objective (Nikon CF175 LWD 16xW) based on a previous design (Rosenegger et al., 2014). The orientation of the 2P microscope objective was adjustable and was oriented perpendicular to the cranial window.

Two-photon excitation of GCaMP6f and Texas Red dextran was achieved using a Ti:sapphire laser (Chameleon Vision, Coherent) tuned to 930 nm (30 to 65 mW post-objective laser power). Fluorescence was detected using bandpass emission filters (GCaMP6f, Chroma ET525/50m; Texas Red, Chroma ET630/75m) and GaAsP photomultiplier tubes (H10770PA-40; Hamamatsu). Images (256 × 256 pixels) were acquired at 4.25Hz. Additional trials were acquired at 8.41Hz (256 × 256 pixels) to investigate the presence of fast Ca^{2+} events.

Blood vessel selection, classification, and imaging

Penetrating arteries that responded to air puffs with dilations were identified and their vascular trees were chosen for imaging. Penetrating arterioles were classified as zero order vessels while capillaries were classified as follows: vessels branching off the penetrating arteriole were considered 1^{st} order capillaries, branches off 1^{st} order capillaries as 2^{nd} order capillaries, and so forth up to 4^{th} order capillaries. Vessels were imaged in multiple trials consisting of a 10 s pre-stimulus period, a 500 ms air puff onto the contralateral whiskers, and a 6.5 s post-stimulus period. Imaged vessels were 70 to 200 μm beneath the cortical surface. Imaging sometimes allowed for multiple vessel orders to be visualized at the same time. In most cases, however, vessels were imaged starting with penetrating arterioles, and continued down through 4^{th} order capillaries. If there were multiple 2^{nd} order vessels, the 3^{rd} and 4^{th} order vessels off of that 2^{nd} order would be imaged before moving onto other 2^{nd} order vessels and its daughter branches. This sequence of imaging a penetrating arteriole and it daughter branches was repeated up to four times during the course of an experimental session. Mouse behavior was monitored during each trial with an IR camera (Thor Labs) to track activity. Trials were sorted according to the behavior observed: running during the pre-stimulus period, running after stimulus presentation, or no running. Trials with running during the pre-stimulus period were discarded. Running trials were not further sorted for speed, acceleration, or duration of running.

Vessel diameter and astrocyte Ca^{2+} signaling measurements

Vessel diameter and astrocyte Ca^{2+} signaling were monitored simultaneously in individual trials, with vessels labeled with Texas Red dextran and astrocytes labeled with GCaMP6f. Time stacks of 2P microscopy images from single trials were registered using a custom

MATLAB (MathWorks) program to correct for motion during trials. Trials with large motion artifacts were discarded.

Vessel diameter was determined in each image by measuring the intensity profile of Texas Red dextran fluorescence along a line drawn perpendicular to the vessel and was taken as the full width at half-maximal intensity of the profile. Plots of vessel diameter versus time from individual trials were then averaged together for all trials on a single vessel with the same category of mouse activity (no running or running after air puff). Typically, three to seven trials from the same activity category were averaged. Vessel responses were measured from these averaged traces. Peak vessel dilation was calculated as

$$100 * (D_{Peak} - D_{Baseline}) / D_{Baseline}$$

where $D_{Baseline}$ is the mean vessel diameter during the last 4 s of the pre-stimulus period and D_{Peak} is the mean of the largest vessel diameter value and the two values immediately preceding and following the maximal value in a 3.5 s window following the stimulus. The latency to the onset of vessel dilation was determined as the time at which the vessel diameter increase surpassed 10% of the peak dilation.

Astrocyte endfoot Ca^{2+} increases were measured within manually drawn regions of interest (ROIs) using ImageJ (Schindelin et al., 2012). The ROIs encompassed the endfeet surrounding that portion of the vessel where vessel diameter was measured and extended approximately 5 μm along the length of the vessel and 2 μm laterally away from the vessel. Calcium increases were also measured in astrocyte fine processes near imaged vessels. ROIs were drawn on both sides of an imaged vessel and encompassed processes beginning ~7 μm from the vessel edge and extending another 10 to 30 μm away from the vessel, depending on the vessel position in the image frame. Plots of GCaMP6f fluorescence intensity vs. time from the same trials used to measure vessel diameter were averaged together. Peak Ca^{2+} responses (ΔF/F) were calculated as

$$(F_{Peak} - F_{Baseline}) / F_{Baseline}$$

where $F_{Baseline}$ is the mean baseline GCaMP6f fluorescence over the 10s pre-stimulus period and F_{Peak} is the mean of the largest fluorescence intensity value and the two values immediately preceding and following it. The latency to the onset of the Ca^{2+} increase was determined as the time at which the fluorescence increase surpassed 10% of the peak fluorescence value.

Statistics

Two sample t-tests and one-way or two-way ANOVAs were used, as appropriate. The sample size (n) for each experiment using Cyto-GCaMP6f animals is reported in Tables 1 to 4 and represents the number of vessels and associated astrocytes sampled. n is otherwise specified in the text. Peak vessel dilations and peak Ca^{2+} responses within a given vessel order were compared using two-way ANOVAs and the Tukey-Kramer post-hoc test separating groups by genotype and activity condition. Two sample t-tests

were used to analyze differences between the WT and IP3R2 KO peak Ca^{2+} responses at capillary endfeet and surrounding processes of a given GCaMP6f condition. The Pearson's correlation coefficient and coefficient of determination (R^2) for capillary dilations and peak Ca^{2+} increases were carried out on both GCaMP6f conditions. Dilation onset latency was analyzed using one-way ANOVAs and the Tukey-Kramer post-hoc test to compare latency differences between orders within a genotype condition. Onset latency to evoked Ca^{2+} increase was analyzed with one-way ANOVAs and the Tukey-Kramer post-hoc test to compare differences between vessel orders within a GCaMP6f condition. Onset latency data for dilation and evoked Ca^{2+} were pooled and compared between the appropriate conditions using two sample t-tests. Evoked Ca^{2+} onset latency cumulative frequency was compared using a two sample Kolmogorov-Smirnov test. Data are expressed as means ± SEM. Significance thresholds were: *$p < 0.05$, **$p < 0.01$, ***$p < 0.001$.

RESULTS

We investigated the relation between astrocyte Ca^{2+} signaling and the dilation of capillaries and arterioles in the somatosensory cortex of the awake mouse. Astrocyte Ca^{2+} signaling was monitored by viral transfection of the genetically encoded Ca^{2+} indicator GCaMP6f while the diameter of blood vessels was measured by labeling vessel lumens with Texas Red dextran. Calcium signaling was measured with the cytoplasmic genetically encoded Ca^{2+} indicator Cyto-GCaMP6f as well as with the membrane-tethered indicator Lck-GCaMP6f. Blood vessel diameter and Ca^{2+} signaling in adjacent astrocyte endfeet and processes were monitored simultaneously with 2P microscopy. Individual penetrating arterioles (zero order vessels) and 1st through 4th order capillaries (Fig. 1a) were monitored in separate trials while astrocyte Ca^{2+} signaling was measured in ROIs adjacent to the vessel (Fig. 1d). In a typical trial, stimulation of the contralateral whiskers produced a short latency vessel dilation followed by an increase in endfoot Ca^{2+} whose onset and peak trailed the vessel dilation (Fig 1b to e).

Trials were divided into a number of groups. Results were separated into trials by different order vessels: zero order penetrating arterioles and 1st, 2nd, 3rd and 4th order capillaries (Dalkara et al., 2011). Results were further separated into trials where the mouse did not run during the trial and trials where the mouse began running following the stimulus. Finally, experiments were performed on WT mice and on IP3R2 KO littermates.

Averaged responses from 4th order capillaries using the cytoplasmic Ca^{2+} indicator are shown in Fig. 2, with results separated into four groups: trials where WT mice did not run, trials where WT mice ran after the onset of the stimulus, trials from IP3R2 KO mice where the mouse did not run, and trials from IP3R2 KO mice where the mouse ran after stimulus onset. In WT mice that did not run (Fig. 2a), whisker stimulation evoked a large, rapid vessel dilation. Astrocyte Ca^{2+} increases, in contrast, were substantially slower, both in onset and in time course. Voluntary running induces the release of norepinephrine, elicits astrocyte Ca^{2+} signaling via α_1 adrenergic activation, and enhances astrocyte sensitivity to local circuit activity (Nimmerjahn et al., 2009; Paukert et al., 2014). In agreement with these findings, we found that astrocyte Ca^{2+} increases were substantially larger in amplitude and longer in duration in trials where the stimulus evoked running (Fig. 2b). However, vessel

dilation in these trials had a similar time course and amplitude to the no running trials. In IP3R2 KO mice (both no running and running trials; Fig. 2c and d), similar amplitude vessel dilations were also seen. However, the astrocyte Ca^{2+} increase was almost abolished. Thus, in all four groups, whisker stimulation evoked similar vessel dilations despite the widely varying Ca^{2+} increases in the astrocyte endfeet contacting the capillaries.

Summaries of all the results using the cytoplasmic Ca^{2+} indicator are given in Fig. 3 and Tables 1 to 4. Several features should be noted. In capillaries of 2nd through 4th orders, there were significant differences in astrocyte Ca^{2+} signaling between trials where mice did not run and where whisker stimulation evoked running (with a mean latency to running onset of 0.62 ± 0.02 s following the initiation of the stimulus; n = 707 trials). Astrocyte Ca^{2+} increases were substantially larger in trials where mice ran, particularly in astrocyte endfeet surrounding the higher order vessels. In 4th order capillaries, for instance, Ca^{2+} increases were 275 ± 39% larger in running trials. In addition, endfoot Ca^{2+} levels remained elevated longer in running trials. This is illustrated in Fig 2b and by the “Latency to Peak Ca^{2+} Increase” in Tables 1 and 3. Despite these large differences in endfoot Ca^{2+} signaling, however, vessel dilations were no larger in running trials than in trials without running.

The opposite was seen in trials on IP3R2 KO mice. For vessels of all orders, evoked astrocyte Ca^{2+} increases were substantially smaller in IP3R2 KO animals (both running and no running trials) than in WT littermates. Indeed, averaged over vessels of all orders, endfoot Ca^{2+} increases were reduced to 9% of WT in KO animals. Despite these dramatic decreases in astrocyte Ca^{2+} signaling, there was only one condition where vessel dilation was reduced between WT and KO animals (2nd order WT Running and IP3R2 KO).

Astrocyte Ca^{2+} increases may be better correlated with the time course of return of vessel diameter back to baseline diameter following its peak rather than to the amplitude of the peak dilation (Girouard et al., 2010; Rosenegger et al., 2015; Gu et al., 2018; Tran et al., 2020). We tested this by determining the time to 50% decay from peak dilation for all vessels that dilated at least 3%. We found that there were no significant differences in the decay time between any of the groups (WT and KO; no running and running) for each vessel order (one-way ANOVAs, Tukey-Kramer post-hoc test, $p > 0.3$).

The astrocyte Ca^{2+} increases summarized in Fig. 3 and in Tables 1 to 4 were measured with the Ca^{2+} indicator Cyto-GCaMP6f. This indicator measures Ca^{2+} levels in the bulk cytoplasm and largely reflects Ca^{2+} released from internal stores (Holtzclaw et al., 2002). This is in accordance with the dramatic decrease in evoked Ca^{2+} signaling observed in IP3R2 KO mice, where the Ca^{2+} release channels in the endoplasmic reticulum are absent. However, astrocyte Ca^{2+} increases can also arise from Ca^{2+} influx across the plasma membrane through P2X1, P2X5, TRPA1 channels, and Ca^{2+}-permeable AMPA receptors (Shigetomi et al., 2013b; Srinivasan et al., 2015; Bazargani and Attwell, 2016; Mishra et al., 2016). It is possible that the cytoplasmic Ca^{2+} indicator did not detect these signals in the KO animals.

We tested whether significant Ca^{2+} activity remained in KO animals by monitoring evoked Ca^{2+} signaling with the membrane-tethered indicator Lck-GCaMP6f, which is sensitive to

Ca^{2+} increases arising from influx across the plasma membrane (Srinivasan et al., 2016). Calcium responses measured from WT and IP3R2 KO animals using the cytoplasmic Ca^{2+} indicator are replotted in Fig. 4a with data from the four orders of capillaries combined (no running trials only). The large decrease in the Ca^{2+} response in the KO animals is evident, with response amplitude dropping from 0.58 ± 0.07 to 0.050 ± 0.004 ΔF/F; only 8.7% of the WT response remained in the KO animals. An average of the Ca^{2+} responses from the four orders of capillaries measured using the membrane-tethered indicator are shown in Fig. 4b. There is a similar, although smaller reduction in the Ca^{2+} responses seen in the KO animals, with response amplitude dropping from 0.26 ± 0.02 to 0.079 ± 0.004 ΔF/F; only 30.2% of WT amplitude remained in the KO animals. Results are summarized in Fig. 4c, showing the large reduction in evoked Ca^{2+} signaling in IP3R2 KO animals using both the cytoplasmic and membrane-tethered GCaMP6f Ca^{2+} indicators.

If astrocyte Ca^{2+} increases contribute to stimulus-evoked capillary dilation, there should be a correlation between the magnitude of the dilation and the size of the evoked-Ca^{2+} increase. We tested this by plotting peak capillary dilation vs. peak endfoot Ca^{2+} increases in WT animals for individual vessels for both Cyto- and Lck-GCaMP6f Ca^{2+} indicators (Fig. 4d). The correlation was extremely weak for both indicators, with R^2 coefficients of determination of 0.048 and 0.001 for the Cyto- and Lck-GCaMP6f Ca^{2+} indicators, respectively. Indeed, for the Lck Ca^{2+} indicator, the correlation trended towards a negative value, the opposite of what one would predict if astrocyte Ca^{2+} mediated vessel dilation.

Calcium events at astrocyte endfeet are commonly associated with astrocyte-mediated vessel dilation (Girouard et al., 2010; MacVicar and Newman, 2015; Biesecker et al., 2016; Boulay et al., 2017; Tran et al., 2018). It is possible, however, that fine astrocyte processes, which are closely associated with synapses and display Ca^{2+} events, may also contribute to vessel dilation by generating and/or releasing vasoactive molecules. Calcium signaling in these fine processes may be retained in IP3R2 KO animals and may evoke vessel dilation. We tested this by determining whether IP3R2 KO animals maintained their evoked Ca^{2+} responses or whether the responses were reduced, as they are at the endfeet. Calcium responses to whisker stimulation were measured in WT and IP3R2 KO animals using the membrane tethered Lck-GCaMP6f Ca^{2+} indicator, which provides a better measure of Ca^{2+} responses than the Cyto indicator in fine processes (Shigetomi et al., 2013a; Srinivasan et al., 2016; Stobart et al., 2018). The mean Ca^{2+} responses around 0 order penetrating arterioles and around 1st through 4th order capillaries are shown in Fig. 5a and b, respectively. Significant reductions in the Ca^{2+} responses are seen in the processes of KO animals, compared to WT. Mean Ca^{2+} response amplitude in processes surrounding arterioles dropped from 0.15 ± 0.02 to 0.07 ± 0.01; only 47% of the WT signal remained in the KO animals. Similarly, Ca^{2+} response amplitude in processes surrounding capillaries dropped from 0.16 ± 0.01 to 0.07 ± 0.003; only 44% of the WT signal remained in the KOs. These reductions are similar to the reductions seen in endfeet when measured with the Lck-GCaMP6f Ca^{2+} indicator (Fig. 4b). The results are summarized in Fig. 5c, and show a substantial reduction in evoked Ca^{2+} signaling in the astrocyte processes of IP3R2 KO animals, around both 0 order penetrating arterioles and around capillaries.

Latencies to the onset of vessel dilation in different order vessels are summarized in Fig. 6, where results from no running trials are displayed. There were no significant differences to onset of dilation between WT and IP3R2 KO animals (two sample t-test of combined WT vs combined IP3R2 KO trials, $p = 0.1$). In WT animals, onset latencies were shorter for 1st order capillaries compared to arterioles and higher order capillaries (0 order vs 1st order onset latency, $p = 0.026$; 1st order vs 2nd order onset latency, $p = 0.009$. 1-way ANOVA, Tukey-Kramer post-hoc test used for other WT order comparisons, $p > 0.05$).

Latencies to the onset of endfoot astrocyte Ca^{2+} increases are summarized in Fig. 7. For Ca^{2+} increases in the cytoplasm of astrocyte endfeet (measured with Cyto-GCaMP6f), mean latencies were similar for endfeet contacting all orders of capillaries, approximately 1.3 s, and somewhat shorter for endfeet contacting arterioles (Fig. 7a) (1-way ANOVA, Tukey-Kramer post-hoc test Cyto-GCaMP6f order comparisons, all comparisons had $p > 0.75$). There was a wide distribution of latencies within all groups, with latencies as short as 0.15 s seen in all vessel orders. We also measured endfoot Ca^{2+} signaling using Lck-GCaMP6f to determine whether faster Ca^{2+} signals were generated near the plasma membrane (Srinivasan et al., 2016). Indeed, mean latencies for endfoot Ca^{2+} signaling were shorter for all vessel orders when monitored with Lck-GCaMP6f (two sample t-test of combined Cyto-GCaMP6f ($n = 117$) vs combined Lck-GCaMP6f ($n = 65$) trials, $p = 9 \times 10^{-6}$). Latencies as short as 0.15 s were observed with Lck-GCaMP6f as well. A comparison of endfoot Ca^{2+} response latencies monitored with cytoplasmic and membrane-tethered GCaMP6f is shown in heat map and cumulative frequency plots (Fig. 7b to d). Short latency responses are seen with both cytoplasmic and membrane-tethered indicators. On average, Ca^{2+} signaling near the plasma membrane had shorter latencies than did cytoplasmic Ca^{2+} signals (two sample Kolmogorov-Smirnov test, $p = 1.25 \times 10^{-4}$).

Astrocyte Ca^{2+} responses were monitored with a 2P microscopy acquisition rate of 4.25 Hz, which limits the temporal resolution of Ca^{2+} latency measurements. In order to determine whether shorter latency Ca^{2+} responses occurred, experiments were also conducted using a 2P microscopy frame rate of 8.41 Hz. No shorter latency responses were observed at these faster acquisition rates (two sample t-test of combined Lck-GCaMP6f at 4.25Hz ($n = 38$) vs combined Lck-GCaMP6f at 8.41Hz ($n = 27$), $p = 0.08$).

DISCUSSION

We have investigated the role of astrocyte Ca^{2+} signaling in mediating neurovascular coupling in penetrating arterioles and capillaries in the cerebral cortex. There is no question as to whether Ca^{2+} increases in astrocytes can result in the dilation of both arterioles and capillaries. Both types of vessels dilate when Ca^{2+} concentrations are raised in astrocytes by photolysis of caged Ca^{2+} or IP_3 (Metea and Newman, 2006; Takano et al., 2006; Gordon et al., 2008; Girouard et al., 2010; Mishra and Newman, 2010). The question we address here is whether astrocyte Ca^{2+} increases mediate vessel dilation in vivo under physiological conditions.

The role of astrocyte Ca^{2+} signaling in mediating neurovascular coupling has been examined by a number of laboratories in the past. Many investigators have concluded that the dilation

of penetrating arterioles is not mediated by Ca^{2+} increases in astrocyte endfeet (Bonder and McCarthy, 2014; Hill et al., 2015; Institoris et al., 2015; Mishra et al., 2016). However, relatively few studies have examined the causal relation between astrocyte Ca^{2+} increases and the dilation of capillaries (Biesecker et al., 2016; Mishra et al., 2016; Lind et al., 2018; Tran et al., 2018).

Previously, Mishra et al (2016) concluded that capillary but not arteriole dilation in the cerebral cortex is mediated by Ca^{2+} increases in astrocytes. Similarly, Biesecker et al (2016) concluded that capillary but not arteriole dilation in the retina is mediated by Ca^{2+} increases in Müller cells, the principal macroglial cells of the retina.

Given these previous findings, we anticipated that capillary dilation in the cortex of the unanesthetized mouse would also be mediated by Ca^{2+} increases in astrocyte endfeet. To our surprise, we found the opposite result. Dilation of capillaries as well as penetrating arterioles were not dependent on Ca^{2+} increases in the endfeet of astrocytes contacting the vessels (Figs. 2 to 3, Tables 1 to 4). Capillary dilations in 1st through 4th order capillaries were, with one exception, not diminished in IP3R2 KO animals, compared to WT littermates, even though evoked Ca^{2+} increases in astrocyte endfeet were reduced to an average of 9% of the WT values. Similarly, capillary dilations were not increased in animals where the whisker stimulus evoked running, even though astrocyte Ca^{2+} signaling increased an average of 240%.

The above observations were made with the cytoplasmic Ca^{2+} indicator Cyto-GCaMP6f. It is well known, however, that astrocyte Ca^{2+} signaling is not completely eliminated in IP3R2 KO animals. Other sources of Ca^{2+}, including additional IP3R isoforms (Sherwood et al., 2017) and surface channels, including P2X1,P2X5, TRPA1 channels, and Ca^{2+}-permeable AMPA receptors (Lalo et al., 2008; Shigetomi et al., 2013b; Srinivasan et al., 2015; Bazargani and Attwell, 2016; Mishra et al., 2016) can also generate astrocyte Ca^{2+} increases. It is possible that Ca^{2+} influx through plasma membrane channels is a more important source for a Ca^{2+}-mediated astrocyte signaling mechanism, as Mishra et al (2016) suggest. This is a reasonable supposition as Ca^{2+}-dependent PLA2 and PLD2 enzymes, which contribute in the synthesis of the vasodilating molecules PGE_2 and EETs, are associated with the plasma membrane (Klein, 2005; Sun et al., 2005, p 1). Similarly, BK channels, which are activated by Ca^{2+} and release vasodilating K^+, are imbedded in the plasma membrane (Ledoux et al., 2006).

With this in mind, we evaluated the importance of Ca^{2+} influx through plasma membrane channels by measuring whisker stimulation-evoked Ca^{2+} increases using the membrane-tethered Ca^{2+} indicator Lck-GCaMP6f. Our results were similar to those obtained with the cytoplasmic indicator. Evoked Ca^{2+} increases at endfeet were reduced to 30% of WT values in IP3R2 KO mice. Another potential source of Ca^{2+} signaling and vasoactive molecule production are the fine astrocyte processes that are associated with synapses. Calcium signals within these processes near capillaries were also reduced, in this case to 44% of WT values, in IP3R2 KO animals, confirming that the reduction in stimulus-evoked Ca^{2+} responses is preserved within astrocyte processes as well as endfeet. Although this is a smaller reduction than seen with Cyto-GCaMP6f, it is nevertheless substantial and one

would expect to see some reduction in evoked capillary dilation if the dilation was at all dependent on astrocyte Ca^{2+} signaling, a reduction we did not see.

Another test of the dependence of capillary dilation on astrocyte Ca^{2+} signaling is to evaluate the correlation between the two. If capillary dilation was dependent on astrocyte Ca^{2+} signaling, one would expect to see a positive correlation between Ca^{2+} increases and dilation. We found, instead, that there was no meaningful correlation between astrocyte Ca^{2+} signaling and capillary dilation for trials using both the cytoplasmic and the membrane-tethered Ca^{2+} indicator (Fig. 4d). Indeed, for the membrane-tethered indicator, which may reflect the more meaningful Ca^{2+} signal for neurovascular coupling, there was a trend towards a negative correlation.

One caveat in our experiments should be noted. The IP3R2 KO animals we used were a constitutive mouse line and compensatory mechanisms may have been induced. Neurovascular coupling pathways other than a Ca^{2+} dependent astrocyte mechanism may have been upregulated to play a more important role in capillary dilation. Although this is a potential confound when interpreting the results of our IP3R2 KO experiments, it cannot account for the observation that capillary dilation was not altered when astrocyte Ca^{2+} signaling increased substantially in WT animals when mice ran.

Our conclusion that capillary dilation is unrelated to astrocyte Ca^{2+} signaling in the cortex conflicts with the conclusions of Mishra et al (2016) and Biesecker et al (2016). There could be several reasons that the findings of Mishra et al (2016) differed from ours. First, their experiments were based on chelation of astrocyte Ca^{2+} with BAPTA in brain slices and purinergic antagonist blockade of Ca^{2+} increases in anesthetized in vivo preparations while our work utilized awake WT and IP3R2 KO animals. Second, they recorded from astrocytes in cortical layers III-VI in their slices while we imaged astrocytes in layers I-III. However, their in vivo recordings were from similar cortical depths as ours. Third, Mishra et al (2016) used electrical stimulation to excite neuronal activity while we used air puff whisker stimulation. It is possible that electrical stimulation caused larger increases in neuronal activity, leading to the activation of astrocytic P2X1 receptors, while our physiological stimulus did not. If this were the case, one might conclude that astrocyte Ca^{2+} signaling can contribute to capillary neurovascular coupling, but only for non-physiological stimuli that evoke greater than normal increases in neuronal activity.

Biesecker et al (2016) characterized neurovascular coupling in the retina utilizing IP3R2 KO animals. Mechanisms of neurovascular coupling could well differ in different regions of the CNS. Indeed, capillary dilation in the olfactory bulb may be mediated by astrocyte Ca^{2+} signaling, as stimulus-evoked Ca^{2+} increases in astrocyte processes consistently precede capillary dilations in the olfactory bulb (Otsu et al., 2015; Rungta et al., 2018).

If capillary dilation is not mediated by astrocyte Ca^{2+} signaling in the cortex, what signaling mechanism mediates dilation? Our experiments do not address this question. However, there are numerous neurovascular coupling mechanisms that could mediate capillary dilation. Dilation could be mediated by release of prostaglandins and NO directly from neurons. Dilation could also be mediated by vasodilating agents released from astrocytes in a non-

Ca^{2+}-dependent manner. We previously proposed that astrocytes could release PGE_2 and EETs derived from arachidonic acid originating from neurons (Nippert et al., 2018). This mechanism of astrocyte signaling does not depend on astrocyte Ca^{2+} activity. Dilation could also be mediated by K^+ release from astrocytes by K^+ siphoning (Paulson and Newman, 1987).

Active capillary dilation is thought to contribute substantially to the overall increase in cerebral blood flow that occurs during functional hyperemia (Hall et al., 2014; Gould et al., 2017). Yet some have questioned whether capillaries are capable of actively dilating, based on the observation that pericytes surrounding capillaries do not contain the contractile proteins necessary for capillary contraction and relaxation (Hill et al., 2015). Several subsequent studies have shown, however, that pericytes, even those contacting 7th order capillaries, do contain the contractile protein α-smooth muscle actin (Alarcon-Martinez et al., 2018, 2019). Many physiological studies have also demonstrated that pericytes surrounding capillaries can contract and that capillaries can actively constrict and dilate (Puro, 2007; Hall et al., 2014; Kornfield and Newman, 2014; Biesecker et al., 2016; Mishra et al., 2016; Kisler et al., 2017; Cai et al., 2018). The present results confirm this finding. We found that capillaries up though the 4th order show large dilations in response to a natural physiological stimulus. In addition, 1st order capillaries dilate before upstream arterioles (Fig. 6, Table 1), a finding that has been reported by several other laboratories (Hall et al., 2014; Cai et al., 2018; Rungta et al., 2018; Grubb et al., 2020). This could not occur if capillary dilation was the result of passive stretch due to an increase in perfusion pressure generated by the dilation of upstream arterioles. We also found that 2nd through 4th order capillaries dilate with approximately the same latency as penetrating arterioles.

The existence of short latency Ca^{2+} increases in astrocytes has also been controversial. Several studies have observed stimulus-evoked Ca^{2+} increases in astrocytes with latencies significantly shorter than the latency of vessel dilation (Otsu et al., 2015; Lind et al., 2018; Stobart et al., 2018). Our results confirm these observations. We see evoked Ca^{2+} increases in astrocyte endfeet with latencies as brief as 0.15 s, similar to latencies observed previously (Lind et al., 2013; Stobart et al., 2018). This observation does not demonstrate that these rapid Ca^{2+} increases are causing capillary dilation, however.

In summary, we have demonstrated that capillary as well as arteriole dilation in the cerebral cortex is not related to astrocyte Ca^{2+} increases. Whisker stimulation evokes capillary dilations of similar amplitudes in WT and IP3R2 KO animals and in animals that are stationary or running, even though astrocyte Ca^{2+} signaling varies widely amongst these different groups. Our findings do not, however, exclude the possibility that astrocyte Ca^{2+} signaling contributes to capillary dilation in other regions of the CNS.

Acknowledgements:

We thank Anusha Mishra for her insightful comments on an earlier version of the manuscript. Supported in part by National Institutes of Health Grants R01-EY-026514, R01-EY-026882, and P30-EY-011374 to E.A.N.

DATA AVAILABILITY STATEMENT.

The data that support the findings of this study are available from the corresponding author upon reasonable request.

References

Alarcon-Martinez L, Yilmaz-Ozcan S, Yemisci M, Schallek J, Kilic K, Can A, Di Polo A, Dalkara T. 2018. Capillary pericytes express alpha-smooth muscle actin, which requires prevention of filamentous-actin depolymerization for detection. Elife 7:e34861. [PubMed: 29561727]

Alarcon-Martinez L, Yilmaz-Ozcan S, Yemisci M, Schallek J, Kilic K, Villafranca-Baughman D, Can A, Di Polo A, Dalkara T. 2019. Retinal ischemia induces alpha-SMA-mediated capillary pericyte contraction coincident with perivascular glycogen depletion. Acta Neuropathol Commun 7:134. [PubMed: 31429795]

Attwell D, Buchan AM, Charpak S, Lauritzen M, MacVicar BA, Newman EA. 2010. Glial and neuronal control of brain blood flow. Nature 468:232–243. [PubMed: 21068832]

Attwell D, Mishra A, Hall CN, O'Farrell FM, Dalkara T. 2016. What is a pericyte? J Cereb Blood Flow Metab.

Bazargani N, Attwell D. 2016. Astrocyte calcium signaling: the third wave. Nat Neurosci 19:182–189. [PubMed: 26814587]

Biesecker KR, Srienc AI, Shimoda AM, Agarwal A, Bergles DE, Kofuji P, Newman EA. 2016. Glial Cell Calcium Signaling Mediates Capillary Regulation of Blood Flow in the Retina. J Neurosci 36:9435–45. [PubMed: 27605617]

Bonder DE, McCarthy KD. 2014. Astrocytic Gq-GPCR-linked IP3R-dependent Ca^{2+} signaling does not mediate neurovascular coupling in mouse visual cortex in vivo. J Neurosci 34:13139–13150. [PubMed: 25253859]

Boulay A-C, Saubaméa B, Adam N, Chasseigneaux S, Mazaré N, Gilbert A, Bahin M, Bastianelli L, Blugeon C, Perrin S, Pouch J, Ducos B, Le Crom S, Genovesio A, Chrétien F, Declèves X, Laplanche J-L, Cohen-Salmon M. 2017. Translation in astrocyte distal processes sets molecular heterogeneity at the gliovascular interface. Cell Discov 3:17005. [PubMed: 28377822]

Cai C, Fordsmann JC, Jensen SH, Gesslein B, Lonstrup M, Hald BO, Zambach SA, Brodin B, Lauritzen MJ. 2018. Stimulation-induced increases in cerebral blood flow and local capillary vasoconstriction depend on conducted vascular responses. Proc Natl Acad Sci U S A 115:E5796–E5804. [PubMed: 29866853]

Dalkara T, Gursoy-Ozdemir Y, Yemisci M. 2011. Brain microvascular pericytes in health and disease. Acta Neuropathol 122:1–9. [PubMed: 21656168]

Girouard H, Bonev AD, Hannah RM, Meredith A, Aldrich RW, Nelson MT. 2010. Astrocytic endfoot Ca^{2+} and BK channels determine both arteriolar dilation and constriction. Proc Natl Acad Sci U A 107:3811–3816.

Goldey GJ, Roumis DK, Glickfeld LL, Kerlin AM, Reid RC, Bonin V, Schafer DP, Andermann ML. 2014. Removable cranial windows for long-term imaging in awake mice. Nat Protoc 9:2515–2538. [PubMed: 25275789]

Gordon GRJ, Choi HB, Rungta RL, Ellis-Davies GCR, MacVicar BA. 2008. Brain metabolism dictates the polarity of astrocyte control over arterioles. Nature 456:745–749. [PubMed: 18971930]

Gould IG, Tsai P, Kleinfeld D, Linninger A. 2017. The capillary bed offers the largest hemodynamic resistance to the cortical blood supply. J Cereb Blood Flow Metab 37:52–68. [PubMed: 27780904]

Grubb S, Cai C, Hald BO, Khennouf L, Murmu RP, Jensen AGK, Fordsmann J, Zambach S, Lauritzen M. 2020. Precapillary sphincters maintain perfusion in the cerebral cortex. Nat Commun 11:395. [PubMed: 31959752]

Gu X, Chen W, Volkow ND, Koretsky AP, Du C, Pan Y. 2018. Synchronized Astrocytic Ca2+ Responses in Neurovascular Coupling during Somatosensory Stimulation and for the Resting State. Cell Rep 23:3878–3890. [PubMed: 29949771]

Hall CN, Reynell C, Gesslein B, Hamilton NB, Mishra A, Sutherland BA, O'Farrell FM, Buchan AM, Lauritzen M, Attwell D. 2014. Capillary pericytes regulate cerebral blood flow in health and disease. Nature 508:55–60. [PubMed: 24670647]

Hill RA, Tong L, Yuan P, Murikinati S, Gupta S, Grutzendler J. 2015. Regional blood flow in the normal and ischemic brain Is controlled by arteriolar smooth muscle cell contractility and not by capillary pericytes. Neuron 87:95–110. [PubMed: 26119027]

Holtzclaw LA, Pandhit S, Bare DJ, Mignery GA, Russell JT. 2002. Astrocytes in adult rat brain express type 2 inositol 1,4,5-trisphosphate receptors. Glia 39:69–84. [PubMed: 12112377]

Institoris A, Rosenegger DG, Gordon GR. 2015. Arteriole dilation to synaptic activation that is sub-threshold to astrocyte endfoot Ca^{2+} transients. J Cereb Blood Flow Metab 35:1411–1415. [PubMed: 26126870]

Khennouf L, Gesslein B, Brazhe A, Octeau JC, Kutuzov N, Khakh BS, Lauritzen M. 2018. Active role of capillary pericytes during stimulation-induced activity and spreading depolarization. Brain 141:2032–2046. [PubMed: 30053174]

Kisler K, Nelson AR, Rege SV, Ramanathan A, Wang Y, Ahuja A, Lazic D, Tsai PS, Zhao Z, Zhou Y, Boas DA, Sakadzic S, Zlokovic BV. 2017. Pericyte degeneration leads to neurovascular uncoupling and limits oxygen supply to brain. Nat Neurosci 20:406–416. [PubMed: 28135240]

Klein J 2005. Functions and pathophysiological roles of phospholipase D in the brain. J Neurochem 94:1473–87. [PubMed: 16042758]

Kornfield TE, Newman EA. 2014. Regulation of blood flow in the retinal trilaminar vascular network. J Neurosci 34:11504–11513. [PubMed: 25143628]

Lalo U, Pankratov Y, Wichert SP, Rossner MJ, North RA, Kirchhoff F, Verkhratsky A. 2008. P2X1 and P2X5 subunits form the functional P2X receptor in mouse cortical astrocytes. J Neurosci 28:5473–5480. [PubMed: 18495881]

Ledoux J, Werner ME, Brayden JE, Nelson MT. 2006. Calcium-activated potassium channels and the regulation of vascular tone. Physiology 21:69–78. [PubMed: 16443824]

Lind BL, Brazhe AR, Jessen SB, Tan FCC, Lauritzen MJ. 2013. Rapid stimulus-evoked astrocyte Ca^{2+} elevations and hemodynamic responses in mouse somatosensory cortex in vivo. Proc Natl Acad Sci U A 110:E4678–E4687.

Lind BL, Jessen SB, Lonstrup M, Josephine C, Bonvento G, Lauritzen M. 2018. Fast Ca(2+) responses in astrocyte end-feet and neurovascular coupling in mice. Glia 66:348–358. [PubMed: 29058353]

MacVicar BA, Newman EA. 2015. Astrocyte regulation of blood flow in the brain. In: Barres BA, Freeman MR, Stevens B, editors. Cold Spring Harb Perspect Biol., Glia. . p 35–48.

Metea MR, Newman EA. 2006. Glial cells dilate and constrict blood vessels: a mechanism of neurovascular coupling. J Neurosci 26:2862–70. [PubMed: 16540563]

Mishra A, Hall CN, Howarth C, Freeman RD. 2021. Key relationships between non-invasive functional neuroimaging and the underlying neuronal activity. Philos Trans R Soc B Biol Sci 376:20190622.

Mishra A, Newman EA. 2010. Inhibition of inducible nitric oxide synthase reverses the loss of functional hyperemia in diabetic retinopathy. Glia 58:1996–2004. [PubMed: 20830810]

Mishra A, Reynolds JP, Chen Y, Gourine AV, Rusakov DA, Attwell D. 2016. Astrocytes mediate neurovascular signaling to capillary pericytes but not to arterioles. Nat Neurosci 19:1619–1627. [PubMed: 27775719]

Nimmerjahn A, Mukamel EA, Schnitzer MJ. 2009. Motor behavior activates Bergmann glial networks. Neuron 62:400–412. [PubMed: 19447095]

Nippert AR, Biesecker KR, Newman EA. 2018. Mechanisms Mediating Functional Hyperemia in the Brain. Neuroscientist 24:73–83. [PubMed: 28403673]

Nizar K, Uhlirova H, Tian P, Saisan PA, Cheng Q, Reznichenko L, Weldy KL, Steed TC, Sridhar VB, MacDonald CL, Cui J, Gratiy SL, Sakadzic S, Boas DA, Beka TI, Einevoll GT, Chen J, Masliah E, Dale AM, Silva GA, Devor A. 2013. In vivo stimulus-induced vasodilation occurs without IP_3 receptor activation and may precede astrocytic calcium increase. J Neurosci 33:8411–8422. [PubMed: 23658179]

Otsu Y, Couchman K, Lyons DG, Collot M, Agarwal A, Mallet JM, Pfrieger FW, Bergles DE, Charpak S. 2015. Calcium dynamics in astrocyte processes during neurovascular coupling. Nat Neurosci 18:210–8. [PubMed: 25531572]

Paukert M, Agarwal A, Cha J, Doze VA, Kang JU, Bergles DE. 2014. Norepinephrine Controls Astroglial Responsiveness to Local Circuit Activity. Neuron 82:1263–1270. [PubMed: 24945771]

Paulson OB, Newman EA. 1987. Does the release of potassium from astrocyte endfeet regulate cerebral blood flow? Science 237:896–898. [PubMed: 3616619]

Pfeiffer T, Li Y, Attwell D. 2021. Diverse mechanisms regulating brain energy supply at the capillary level. Curr Opin Neurobiol 69:41–50. [PubMed: 33485189]

Puro DG. 2007. Physiology and pathobiology of the pericyte-containing retinal microvasculature: new developments. Microcirculation 14:1–10. [PubMed: 17365657]

Rosenegger DG, Tran CH, LeDue J, Zhou N, Gordon GR. 2014. A high performance, cost-effective, open-source microscope for scanning two-photon microscopy that is modular and readily adaptable. PLoS One 9:e110475. [PubMed: 25333934]

Rosenegger DG, Tran CHT, Wamsteeker Cusulin JI, Gordon GR. 2015. Tonic Local Brain Blood Flow Control by Astrocytes Independent of Phasic Neurovascular Coupling. J Neurosci 35:13463–13474. [PubMed: 26424891]

Rungta RL, Chaigneau E, Osmanski BF, Charpak S. 2018. Vascular Compartmentalization of Functional Hyperemia from the Synapse to the Pia. Neuron 99:362–375 e4. [PubMed: 29937277]

Schindelin J, Arganda-Carreras I, Frise E, Kaynig V, Longair M, Pietzsch T, Preibisch S, Rueden C, Saalfeld S, Schmid B, Tinevez J-Y, White DJ, Hartenstein V, Eliceiri K, Tomancak P, Cardona A. 2012. Fiji: an open-source platform for biological-image analysis. Nat Methods 9:676–682. [PubMed: 22743772]

Sherwood MW, Arizono M, Hisatsune C, Bannai H, Ebisui E, Sherwood JL, Panatier A, Oliet SHR, Mikoshiba K. 2017. Astrocytic IP3Rs: Contribution to Ca2+ signalling and hippocampal LTP. Glia 65:502–513. [PubMed: 28063222]

Shigetomi E, Bushong EA, Haustein MD, Tong X, Jackson-Weaver O, Kracun S, Xu J, Sofroniew MV, Ellisman MH, Khakh BS. 2013a. Imaging calcium microdomains within entire astrocyte territories and endfeet with GCaMPs expressed using adeno-associated viruses. J Gen Physiol 141:633–47. [PubMed: 23589582]

Shigetomi E, Jackson-Weaver O, Huckstepp RT, O'Dell TJ, Khakh BS. 2013b. TRPA1 channels are regulators of astrocyte basal calcium levels and long-term potentiation via constitutive D-serine release. J Neurosci 33:10143–10153. [PubMed: 23761909]

Srinivasan R, Huang BS, Venugopal S, Johnston AD, Chai H, Zeng H, Golshani P, Khakh BS. 2015. Ca2+ signaling in astrocytes from Ip3r2−/− mice in brain slices and during startle responses in vivo. Nat Neurosci 18:708–717. [PubMed: 25894291]

Srinivasan R, Lu TY, Chai H, Xu J, Huang BS, Golshani P, Coppola G, Khakh BS. 2016. New Transgenic Mouse Lines for Selectively Targeting Astrocytes and Studying Calcium Signals in Astrocyte Processes In Situ and In Vivo. Neuron 92:1181–1195. [PubMed: 27939582]

Stobart JL, Ferrari KD, Barrett MJP, Gluck C, Stobart MJ, Zuend M, Weber B. 2018. Cortical Circuit Activity Evokes Rapid Astrocyte Calcium Signals on a Similar Timescale to Neurons. Neuron 98:726–735 e4. [PubMed: 29706581]

Sun GY, Xu J, Jensen MD, Yu S, Wood WG, Gonzalez FA, Simonyi A, Sun AY, Weisman GA. 2005. Phospholipase A_2 in astrocytes: responses to oxidative stress, inflammation, and G protein-coupled receptor agonists. Mol Neurobiol 31:27–41. [PubMed: 15953810]

Takano T, Tian GF, Peng W, Lou N, Libionka W, Han X, Nedergaard M. 2006. Astrocyte-mediated control of cerebral blood flow. Nat Neurosci 9:260–7. [PubMed: 16388306]

Takata N, Nagai T, Ozawa K, Oe Y, Mikoshiba K, Hirase H. 2013. Cerebral blood flow modulation by basal forebrain or whisker stimulation can occur independently of large cytosolic Ca^{2+} signaling in astrocytes. PLoS One 8:e66525. [PubMed: 23785506]

Tran CH, Gordon GR. 2015. Acute two-photon imaging of the neurovascular unit in the cortex of active mice. Front Cell Neurosci 9:11. [PubMed: 25698926]

Tran CHT, George AG, Teskey GC, Gordon GR. 2020. Seizures elevate gliovascular unit Ca2+ and cause sustained vasoconstriction. JCI Insight 5.

Tran CHT, Peringod G, Gordon GR. 2018. Astrocytes Integrate Behavioral State and Vascular Signals during Functional Hyperemia. Neuron 100:1133–1148 e3. [PubMed: 30482689]

Main Point

- Prior studies suggested that capillary dilation in the brain required calcium-dependent astrocyte signaling. In contrast, we find that stimulus-evoked capillary dilation in the cerebral cortex is independent of astrocyte calcium signaling.

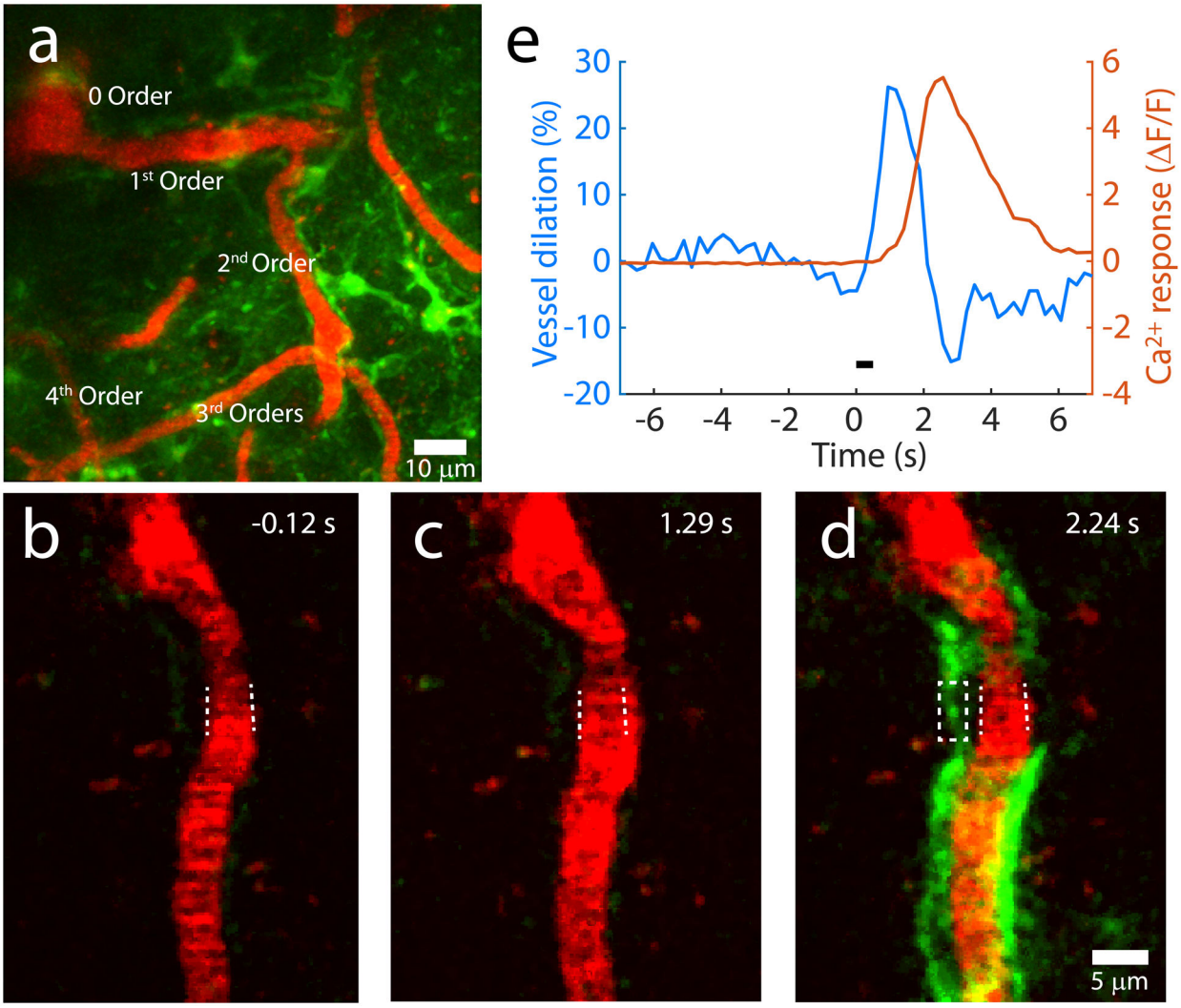

Figure 1.

Measurement of vessel dilation and astrocyte endfoot Ca^{2+} responses. (a) Maximum projection of a Z stack of 2P images showing 0 through 4th order blood vessels in the barrel cortex of the mouse. Vessel are labeled with Texas-Red (red) and astrocytes express Cyto-GCaMP6f (green). (b to d) 2P images from a time series showing dilation of a WT 4th order capillary and Ca^{2+} increases in adjacent endfeet. The hashed lines around the capillary indicate the width of the vessel before stimulation. The time of acquisition, relative to the onset of whisker stimulation, is indicated in each panel. (b) Before stimulation. (c) Near the peak of vessel dilation. (d) Near the peak of the astrocyte Ca^{2+} increase. The boxed area illustrates the ROI used to measure the endfoot Ca^{2+} increase. (e) Traces showing capillary dilation (blue) and astrocyte Ca^{2+} increases (orange) in the trial shown in panels b to d. The traces are an average of 9 no movement trials from the vessel. The black bar indicates the time course of the whisker stimulus.

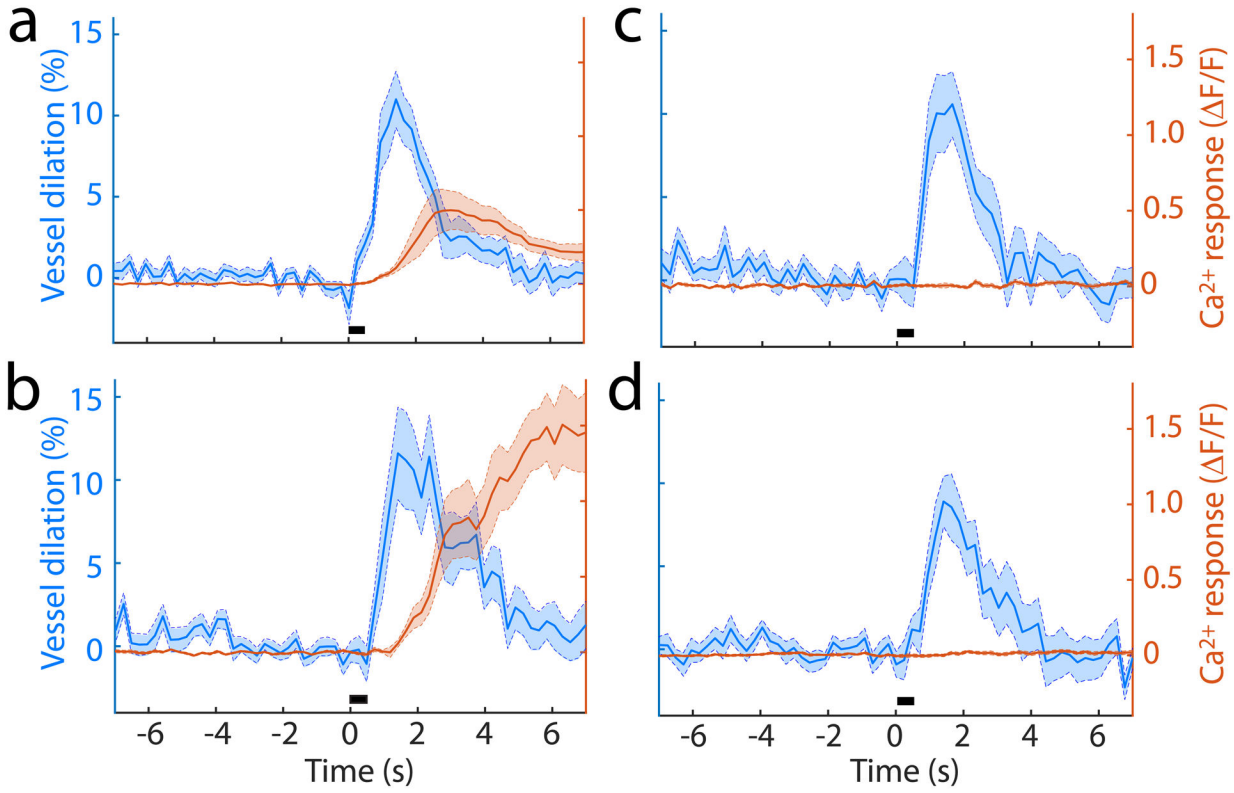

Figure 2.

Average responses of 4th order capillaries and adjacent astrocyte endfeet to whisker stimulation. Mean ± SEM vessel dilations (blue) and astrocyte Ca^{2+} increases (orange) are shown. Black bars indicate the time course of the whisker stimulus. (a) Trials where WT mice did not run. N = 35 vessels. (b) Trials where the stimulus evoked running in WT mice. Running elicited increased astrocyte Ca^{2+} signaling compared to trials where mice did not run. N = 18 vessels. (c) Trials of IP3R2 KO mice where the animal did not run. The evoked astrocyte Ca^{2+} response is largely eliminated compared to WT trials. N = 19 vessels. (d) Trials of IP3R2 KO mice where the stimulus evoked running. N = 22. Despite the widely varying Ca^{2+} responses under the four conditions, vessel dilation remained largely unchanged.

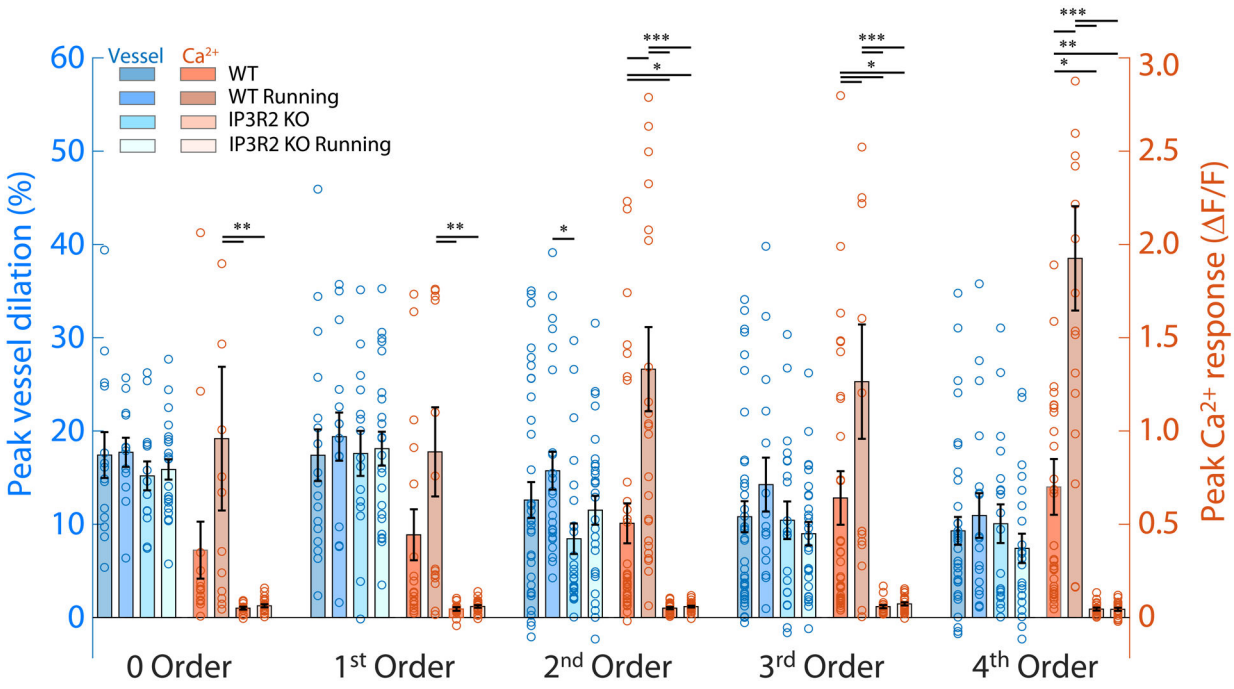

Figure 3.

Summary of vessel dilation and astrocyte endfoot Ca^{2+} responses for all order vessels. Peak vessel dilation (blue) and astrocyte Ca^{2+} increases (orange) for WT, WT Running, IP3R2 KO and IP3R2 KO Running groups for all order vessels are shown as mean ± SEM plus individual vessel values. Astrocyte Ca^{2+} increases displayed are from Cyto-GCaMP6f recordings. Astrocyte Ca^{2+} increases in WT Running trials were significantly larger compared to no running WT trials. Compared to WT and WT Running, astrocyte Ca^{2+} increases in IP3R2 KO groups were significantly decreased. However, across all order vessels, vessel dilations remained largely unchanged despite the increased or decreased astrocyte Ca^{2+} signaling. Two-way ANOVA between genotype and movement conditions for each vessel order, Tukey-Kramer Post Hoc. Between the different orders, both 0 and 1st order vessels (n = 63 and 70, respectively) dilated more than 2nd, 3rd and 4th order vessels (n = 114, 100 and 94, respectively). One-way ANOVA, Tukey-Kramer post-hoc test, $p < 0.05$. * $p < 0.05$, ** $p < 0.01$, *** $p < 0.001$. Tables 1 to 4 contain a summary of the data displayed, including the n's for each category.

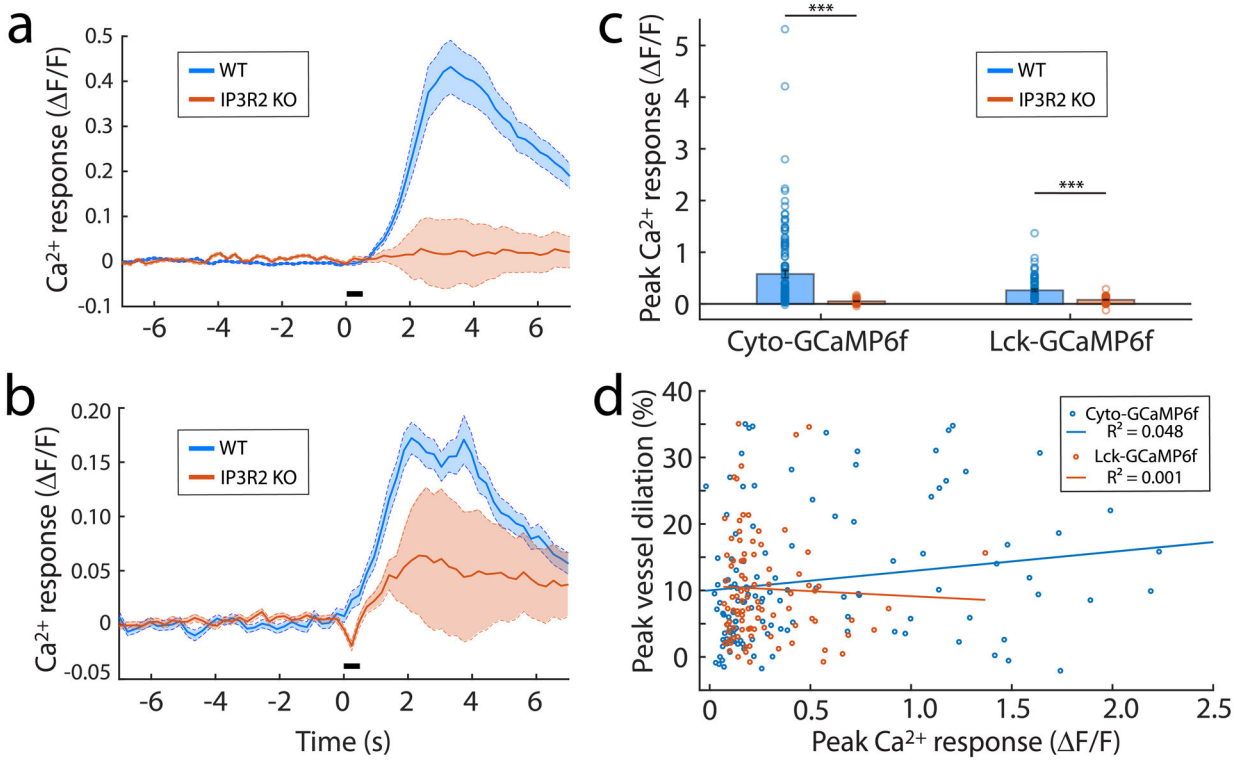

Figure 4.

Astrocyte endfoot Ca^{2+} responses and resulting vessel dilations of 1st through 4th order capillaries. (a) Evoked Ca^{2+} responses in astrocyte endfeet measured with Cyto-GCaMP6f in WT (n = 129) and IP3R2 KO (n = 78) animals. Mean ± SEM of all 1st through 4th order capillary trials. (b) Evoked Ca^{2+} responses in astrocyte endfeet measured with Lck-GCaMP6f in WT (n = 96) and IP3R2 KO (n = 110) animals. Mean ± SEM of all 1st through 4th order capillary trials. (c) Summary of results, showing the decrease of evoked Ca^{2+} responses in IP3R2 KO animals measured with both Cyto- and Lck-GCaMP6f Ca^{2+} indicators. Two sample t-test of WT and IP3R2 KO capillary endfeet peak Ca^{2+} responses, *** $p < 0.001$. (d) Scatterplot showing relation between the evoked astrocyte Ca^{2+} increase and the corresponding capillary dilation for individual capillaries for all 1st through 4th order capillaries. Lines indicate least-squares fit for trials using the Cyto (blue, n = 129) and Lck (orange, n = 96) Ca^{2+} indicators. The R^2 coefficient of determination values are indicated.

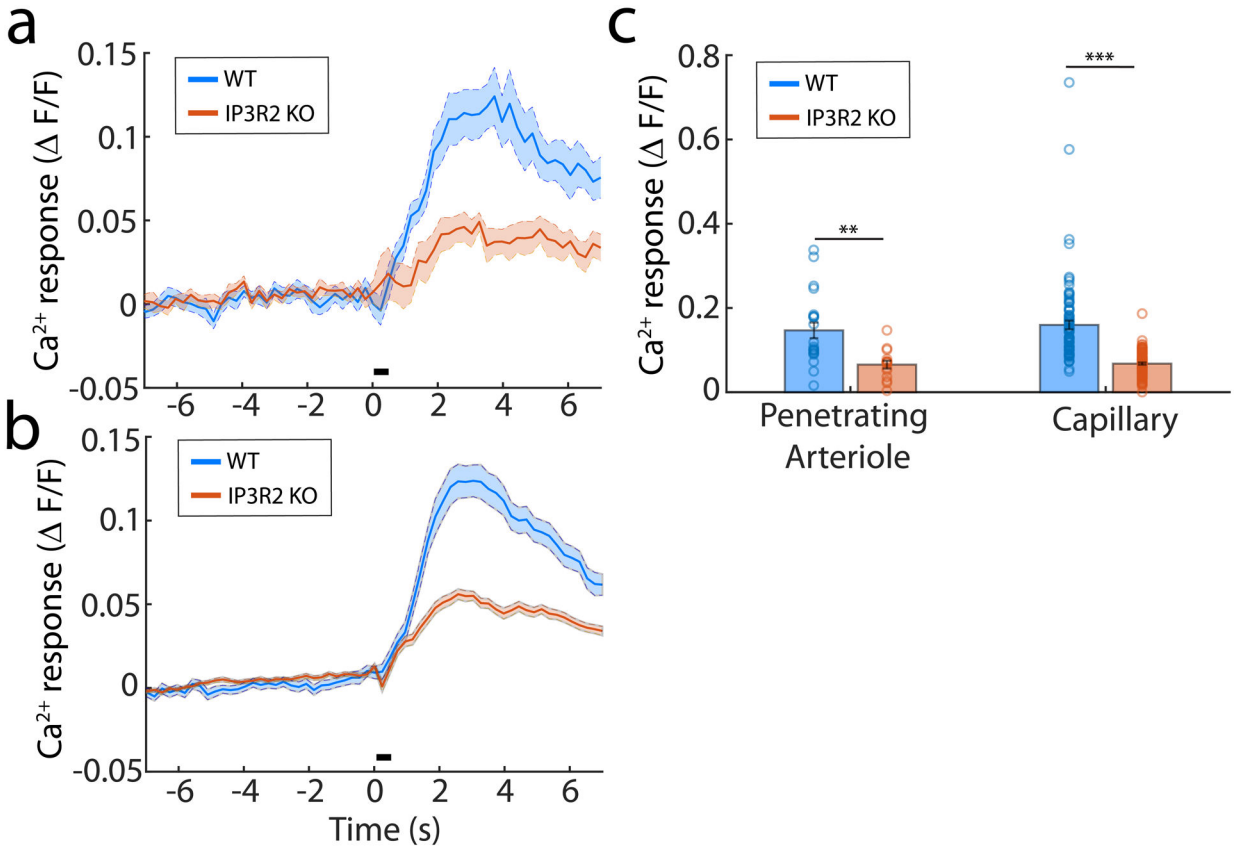

Figure 5.

Astrocyte process Ca^{2+} responses near 0 order penetrating arterioles and 1st through 4th order capillaries. (a) Evoked Ca^{2+} responses in astrocyte processes near 0 order penetrating arterioles measured with Lck-GCaMP6f in WT (n = 21) and IP3R2 KO (n = 15) animals. Mean ± SEM of all Lck-GCaMP6f 0 order trials. (b) Evoked Ca^{2+} responses in astrocyte processes near 1st through 4th order capillaries measured with Lck-GCaMP6f in WT (n = 95) and IP3R2 KO animals (n = 108). Mean ± SEM of all Lck-GCaMP6f 1st through 4th order capillary trials. (c) Summary of results, showing the decrease of evoked Ca^{2+} responses in astrocyte processes near dilating blood vessels. Two sample t-tests of WT and IP3R2 KO animal. ** $p < 0.01$, *** $p < 0.001$.

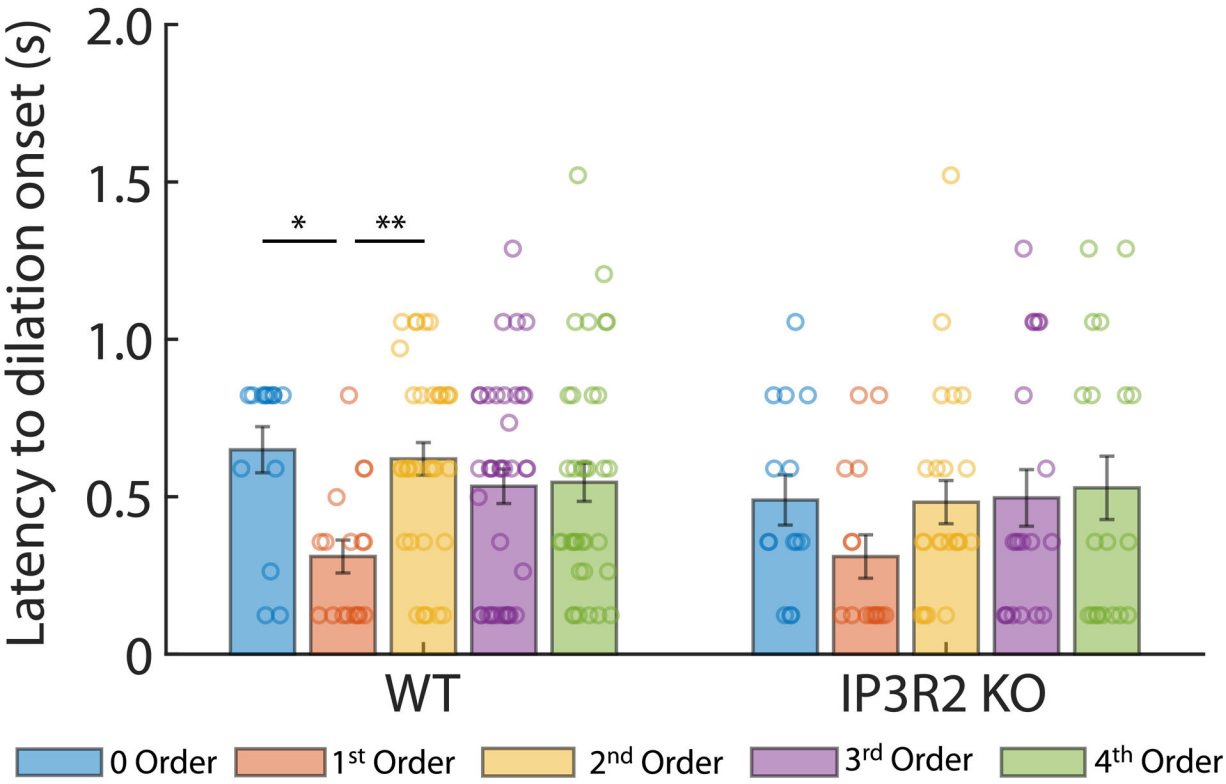

Figure 6.

Latency to the onset of vessel dilation for all order vessels from WT and IP3R2 KO mice trials without running. 1st order capillaries had a faster dilation onset compared to 0 order penetrating arterioles and 2nd order capillaries. One-way ANOVA between the orders of each genotype, Tukey-Kramer Post Hoc. * $p < 0.05$, ** $p < 0.01$. Mean ± SEM plus individual vessels are shown. Tables 1 and 2 contain a summary of the data displayed, including the n's for each category.

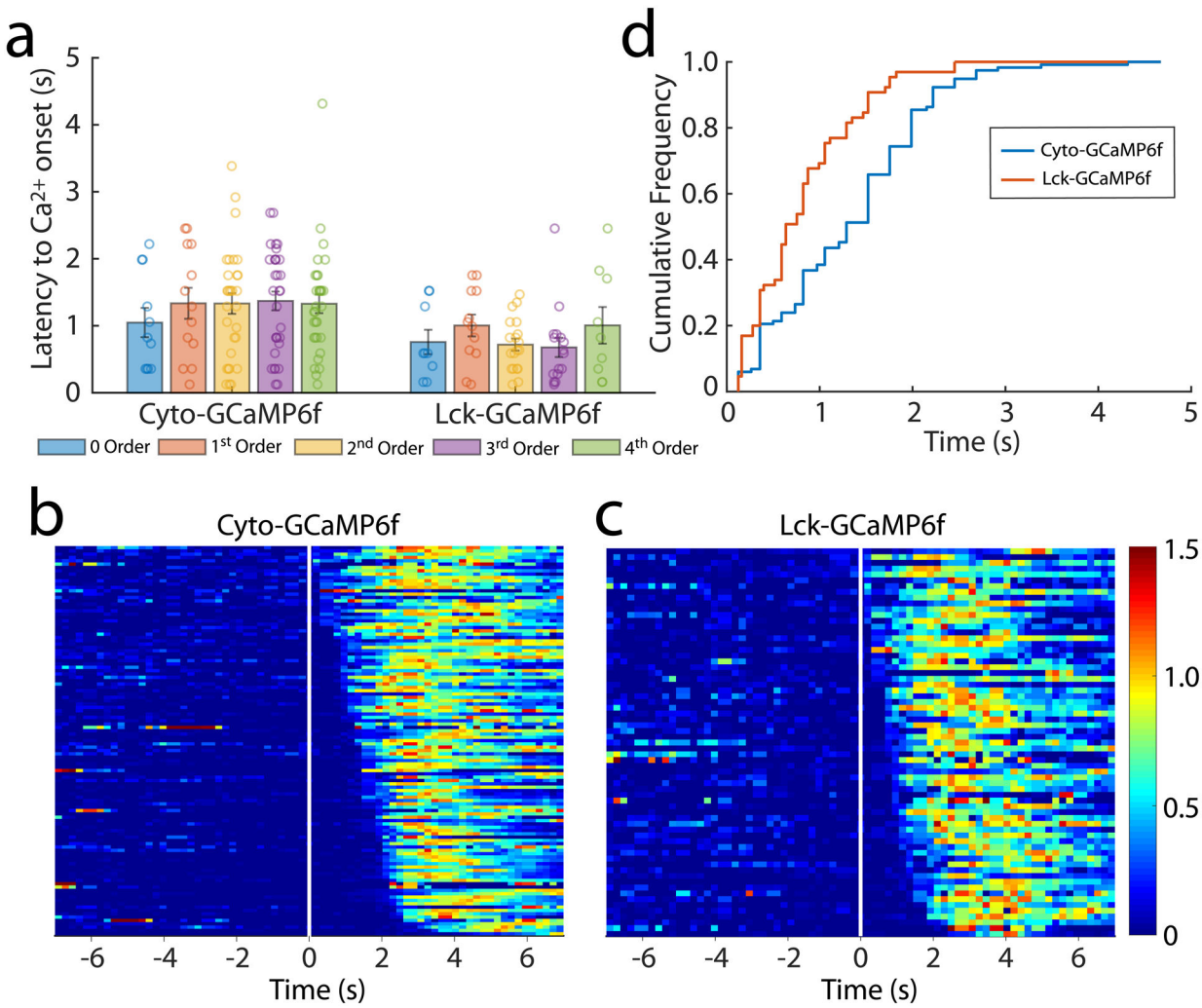

Figure 7.

Latency to the onset of Ca^{2+} increase in astrocyte endfeet contacting vessels of different orders from WT mice trials without running. (a) Summary of latencies for each vessel order of mice expressing either Cyto-GCaMP6f (left, n = 11, 13, 30, 31, 32 for 0, 1st, 2nd, 3rd, 4th orders, respectively) or Lck-GCaMP6f (right, n = 9, 12, 19, 16, 9 for 0, 1st, 2nd, 3rd, 4th orders, respectively). Faster onset latencies were seen in Lck-GCaMP6f trials compared to Cyto-GCaMP6f. Mean ± SEM plus individual vessels are shown. Two sample t-test between onset latency from combined orders of Cyto-GCaMP6f vs Lck-GCaMP6f, $p = 9.0 \times 10^{-6}$. (b & c) Heat maps showing Ca^{2+} responses from astrocyte endfeet contacting individual vessels. Records are sorted by latency. Ca^{2+} signals measured with Cyto-GCaMP6f (b, n = 117) and Lck-GCaMP6f (c, n = 65) are shown. ΔF/F for each vessel was normalized to its peak ΔF/F value. Trials where baseline variation exceeding 30% of peak ΔF/F in the 2 s prior to the stimulus were excluded. Times are relative to stimulus onset (white vertical lines). (d) Cumulative plots of the onset latencies of astrocyte Ca^{2+} responses measured with Cyto-GCaMP6f (blue, n = 117) and Lck-GCaMP6f (orange, n = 65). A greater proportion of

fast Ca^{2+} responses were recorded with Lck-GCaMP6f. Two sample Kolmogorov-Smirnov test, $p = 1.25 \times 10^{-4}$.

Table 1.

Summary of vessel dilation and astrocyte endfoot Ca^{2+} responses in WT animals for trials where the stimulus did not evoke running.

WT	0 Order	1st Order	2nd Order	3rd Order	4th Order
Baseline Diameter (μm)	13 ± 1	5.8 ± 0.4	4.7 ± 0.2	4.4 ± 0.2	4.5 ± 0.2
Peak Dilation (%)	17 ± 3	17 ± 3	13 ± 2	11 ± 2	9.3 ± 1.5
Latency to Onset of Dilation (s)	0.65 ± 0.07	0.31 ± 0.05	0.62 ± 0.05	0.53 ± 0.06	0.55 ± 0.06
Latency to Peak Dilation (s)	1.51 ± 0.07	1.21 ± 0.04	1.5 ± 0.1	1.41 ± 0.07	1.6 ± 0.1
Peak Ca^{2+} Increase (ΔF/F)	0.36 ± 0.15	0.44 ± 0.14	0.51 ± 0.11	0.64 ± 0.14	0.70 ± 0.16
Latency to Onset of Ca^{2+} Increase (s)	0.85 ± 0.2	1.2 ± 0.2	1.3 ± 0.1	1.3 ± 0.1	1.3 ± 0.1
Latency to Peak Ca^{2+} Increase (s)	3.9 ± 0.4	4.1 ± 0.4	3.7 ± 0.3	3.6 ± 0.2	3.7 ± 0.3
n	14	17	35	38	35

Note: The reported sample sizes represent the number of individual vessels measured, which themselves are averages of 3 to 7 trials on that vessel. Ca^{2+} values reported are from Cyto-GCaMP6f animals. Mean ± SEM.

Table 2.

Summary of vessel dilation and astrocyte endfoot Ca^{2+} responses in IP3R2 KO animals for trials where the stimulus did not evoke running.

IP3R2 KO	0 Order	1st Order	2nd Order	3rd Order	4th Order
Baseline Diameter (μm)	13 ± 1	6.3 ± 0.6	4.9 ± 0.3	4.6 ± 0.3	4.3 ± 0.2
Peak Dilation (%)	15 ± 2	18 ± 2	8.4 ± 1.6	10 ± 2	10 ± 2
WT vs IP3R2 KO p-value	0.797	0.999	0.377	0.999	0.990
Latency to Onset of Dilation (s)	0.49 ± 0.08	0.31 ± 0.07	0.48 ± 0.07	0.50 ± 0.09	0.53 ± 0.1
Latency to Peak Dilation (s)	1.4 ± 0.1	1.41 ± 0.08	1.3 ± 0.1	1.2 ± 0.1	1.4 ± 0.1
Peak Ca^{2+} Increase (ΔF/F)	0.050 ± 0.008	0.046 ± 0.010	0.050 ± 0.006	0.058 ± 0.008	0.045 ± 0.008
WT vs IP3R2 KO p-value	0.572	0.132	0.039 *	0.020 *	0.016 *
Latency to Onset of Ca^{2+} Increase (s)	0.59 ± 0.14	0.39 ± 0.09	0.62 ± 0.15	0.41 ± 0.07	0.50 ± 0.12
Latency to Peak Ca^{2+} Increase (s)	3.5 ± 0.5	3.2 ± 0.4	4.1 ± 0.4	3.9 ± 0.5	3.4 ± 0.5
n	14	15	24	20	19

Note: The table includes p-values for comparisons of Peak Dilation and Peak Ca^{2+} increases between WT and IP3R2 KO groups. Ca^{2+} values reported are from Cyto-GCaMP6f animals. Mean ± SEM. 2-way ANOVA, Tukey-Kramer post hoc.

* $p < 0.05$.

Table 3.

Summary of vessel dilation and astrocyte endfoot Ca^{2+} responses in WT animals for trials where the stimulus evoked running.

WT Running	**0 Order**	**1st Order**	**2nd Order**	**3rd Order**	**4th Order**
Baseline Diameter (μm)	14 ± 1.2	5.9 ± 0.5	4.7 ± 0.3	4.7 ± 0.3	4.6 ± 0.3
Peak Dilation (%)	18 ± 1.6	19 ± 2.6	16 ± 2	14 ± 2.9	11 ± 2.4
WT vs WT Running p-value	0.999	0.940	0.606	0.620	0.919
WT Running vs IP3R2 KO p-value	0.754	0.959	0.048 *	0.626	0.990
Latency to Onset of Dilation (s)	0.61 ± 0.08	0.56 ± 0.08	0.47 ± 0.06	0.74 ± 0.13	0.60 ± 0.11
Latency to Peak Dilation (s)	1.5 ± 0.1	1.4 ± 0.1	1.51 ± 0.08	2.0 ± 0.2	2.1 ± 0.2
Peak Ca^{2+} Increase (ΔF/F)	0.96 ± 0.39	0.89 ± 0.24	1.3 ± 0.2	1.3 ± 0.3	1.9 ± 0.3
WT vs WT Running p-value	0.091	0.075	1.43×10^{-05} ***	0.026 *	1.32×10^{-06} ***
WT Running vs IP3R2 KO p-value	0.003 **	1.47×10^{-04} ***	4.67×10^{-09} ***	1.83×10^{-05} ***	3.94×10^{-09} ***
Latency to Onset of Ca^{2+} Increase (s)	1.5 ± 0.3	1.7 ± 0.2	1.9 ± 0.2	2.1 ± 0.3	2.4 ± 0.3
Latency to Peak Ca^{2+} Increase (s)	5.1 ± 0.4	5.3 ± 0.4	5.2 ± 0.3	4.8 ±0.5	4.8 ± 0.4
n	12	15	25	15	18

Note: The table includes p-values for comparisons of Peak Dilation and Peak Ca^{2+} increases between WT and WT Running and between WT Running and IP3R2 KO groups. Ca^{2+} values reported are from Cyto-GCaMP6f animals. Mean ± SEM. 2-way ANOVA, Tukey-Kramer post hoc.

* $p < 0.05$,

** $p < 0.01$,

*** $p < 0.001$.

Table 4.

Summary of vessel dilation and astrocyte endfoot Ca^{2+} responses in IP3R2 KO animals for trials where the stimulus evoked running.

IP3R2 KO Running	0 Order	1st Order	2nd Order	3rd Order	4th Order
Baseline Diameter (μm)	13 ± 1	5.5 ± 0.3	4.6 ± 0.2	4.3 ± 0.2	4.4 ± 0.3
Peak Dilation (%)	16 ± 1	18 ± 2	12 ± 2	9.0 ± 1.3	7.3 ± 1.6
IP3R2 KO vs IP3R2 KO Running p-value	0.989	0.999	0.660	0.953	0.775
WT vs IP3R2 KO Running p-value	0.894	0.996	0.969	0.864	0.863
WT Running vs IP3R2 KO Running p-value	0.855	0.979	0.378	0.300	0.595
Latency to Onset of Dilation (s)	0.59 ± 0.07	0.49 ± 0.08	0.59 ± 0.06	0.66 ± 0.07	0.54 ± 0.08
Latency to Peak Dilation (s)	1.51 ± 0.08	1.31 ± 0.09	1.4 ± 0.1	1.51 ± 0.08	1.9 ± 0.2
Peak Ca^{2+} Increase (ΔF/F)	0.063 ± 0.008	0.059 ± 0.007	0.059 ± 0.005	0.073 ± 0.008	0.044 ± 0.008
IP3R2 KO vs IP3R2 KO Running p-value	1.0	1.0	1.0	1.0	1.0
WT vs IP3R2 KO Running p-value	0.515	0.095	0.028 *	0.011 *	0.010 **
WT Running vs IP3R2 KO Running p-value	0.001 ***	3.78×10^{-05} ***	3.93×10^{-09} ***	6.86×10^{-06} ***	3.82×10^{-09} ***
Latency to Onset of Ca^{2+} Increase (s)	0.45 ± 0.07	0.57 ± 0.14	0.46 ± 0.088	0.58 ± 0.1	0.7 ± 0.2
Latency to Peak Ca^{2+} Increase (s)	4.7 ± 0.4	4.3 ± 0.4	4.1 ± 0.4	4.4 ± 0.4	3.7 ± 0.4
n	23	23	30	27	22

Note: the table includes p-values for comparisons of Peak Dilation and Peak Ca^{2+} increases between IP3R2 KO and IP3R2 KO Running, between WT and IP3R2 KO Running, and between WT Running and IP3R2 KO Running groups. Ca^{2+} values reported are from Cyto-GCaMP6f animals. Mean ± SEM. 2-way ANOVA, Tukey-Kramer post hoc.

* $p < 0.05$,

** $p < 0.01$,

*** $p < 0.001$.